In vivo TssA proximity labeling reveals temporal interactions during Type VI secretion 1 biogenesis and TagA, a protein that stops and holds the sheath.

Yoann G Santin, Thierry Doan, Régine Lebrun, Leon Espinosa, Laure Journet, E. Cascales

In vivo TssA proximity labeling reveals temporal interactions during Type VI secretion biogenesis and TagA, a protein that stops and holds the sheath.

Yoann G. Santin[1], Thierry Doan[1], Régine Lebrun[2], Leon Espinosa[3], Laure Journet[1] & Eric Cascales[1,*]

[1] Laboratoire d'Ingénierie des Systèmes Macromoléculaires, Institut de Microbiologie de la Méditerranée, CNRS UMR7255, Aix-Marseille Université, 31 Chemin Joseph Aiguier, 13402 Marseille Cedex 20, France

[2] Plateforme Protéomique, Marseille Protéomique (MaP) IBiSA labelled, Institut de Microbiologie de la Méditerranée, CNRS, Aix-Marseille Université, 31 Chemin Joseph Aiguier, 13402 Marseille Cedex 20, France.

[3] Plateforme de biophotonique appliquée à la microbiologie, Laboratoire de Chimie Bactérienne, Institut de Microbiologie de la Méditerranée, CNRS UMR7283, Aix-Marseille Université, 31 Chemin Joseph Aiguier, 13402 Marseille Cedex 20, France

* Contact information: cascales@imm.cnrs.fr

The Type VI secretion system (T6SS) is a multiprotein weapon used by bacteria to destroy competitor cells. The T6SS contractile sheath wraps an effector-loaded syringe that is injected into the target cell. This tail structure assembles onto the baseplate that is docked to the membrane complex. In entero-aggregative *Escherichia coli* TssA plays a central role at each stage of the T6SS assembly pathway by stabilizing the baseplate and coordinating the polymerization of the tail. Here we adapted an assay based on APEX2-dependent biotinylation to identify the proximity partners of TssA *in vivo*. By using stage-blocking mutations, we define the temporal contacts of TssA during T6SS biogenesis. This proteomic mapping approach also revealed an additional partner of TssA, TagA. We show that TagA is a cytosolic protein tightly associated with the membrane. Analyses of sheath dynamics further demonstrate that TagA captures the distal end of the sheath to stop its polymerization and to maintain it under the extended conformation.

The bacterial Type VI secretion system (T6SS) is a tail structure that uses a contractile mechanism to inject a molecular syringe loaded with effectors into target cells[1-8]. This sophisticated apparatus is widespread in Gram-negative bacteria, and could be deployed to deliver effectors to the milieu, or into eukaryotic host cells or competitor bacterial cells. The T6SS helps to establish symbiosis, to collect metals or to disable or kill target cells[5,9-13]. At the molecular level, the T6SS requires a minimum set of 12 proteins that are indispensable for its assembly and function whereas additional, accessory proteins such as peptidoglycan-

binding proteins, peptidoglycan remodelling enzymes, disassembly ATPases and spike sharpeners might be necessary to improve its efficiency[4,6,15-17].

The assembly of the T6SS is a coordinated process in which each subunit is recruited in a definite order. The TssA protein is required at each stage of T6SS biogenesis and mediates specific contacts with each of the T6SS sub-complexes[18]. In entero-aggregative *E. coli* (EAEC), the outer membrane lipoprotein TssJ positions first and recruits the inner membrane proteins TssM and TssL[19-21]. Polymerization of the TssJLM heterotrimer into a 1.7-MDa trans-envelope channel, named membrane complex, comprising 10 copies of each protein, occurs after local remodelling of the cell wall which is assured by a transglycosylase that is recruited to and activated by TssM[21,22]. Binding of the TssA protein onto the membrane complex recruits and stabilizes a second multi-protein complex, the baseplate[18]. The baseplate comprises five different proteins: TssE, –F, –G, –K and VgrG[23-26]. The baseplate constitutes the assembly platform for the tail and shares structural and functional homologies with the baseplates of other contractile structures such as bacteriophages[25,26]. The T6SS baseplate is a mosaic structure that groups subunits evolutionarily related to the minimal myophage baseplate (TssE, –F and –G are homologues of the Mu phage Mup46, Mup47 and Mup48 proteins respectively, whereas VgrG is a fusion protein between homologues of Mup44 and Mup45), and TssK, a protein related to siphophage receptor-binding proteins that has evolved a C-terminal domain that anchors the baseplate to the membrane complex[25-30]. Once the baseplate is docked to the membrane complex[23,25,31,32], the tail is built by the processive addition of inner tube and contractile sheath building blocks[3,33-35]. Tail assembly is a coordinated process, in which tube and sheath polymerizations are interdependent but it has been proposed that the assembly of one tube hexamer immediatly precedes the polymerization of one sheath row[18,33]. The coordinated assembly of the sheath with that of the tube is dictated by the TssA subunit[18,36]. During the assembly process, TssA remains at the distal end of the tail, at which new subunits are incorporated[18,37]. Fluorescence microscopy recordings revealed that the length of the tail is not controlled but rather that its polymerization stops once the distal end is at proximity of the membrane[1,2,18,25]. Once the biogenesis of the tail is completed, TssA remains associated to the distal end, and it has been proposed that TssA remains until the last row of sheath contracts[18,36]. However, the molecular mechanism that controls the arrest of sheath polymerization and how the sheath is maintained in the extended conformation for long periods of time are not known.

APEX2-dependent labeling of TssA proximity partners.

Because TssA is located at the distal end of the sheath, we reasoned that definition of the TssA interactome may provide insights onto the late stages of T6SS assembly. To identify TssA partners in living cells, we developed a spatially resolved proteomic-mapping assay based on proximity-dependent biotinylation. APEX2-dependent biotinylation is a recent technology used in eukaryotic cells to define protein sub-cellular localization, membrane protein topology or protein partners[38,39]. APEX2 is an engineered variant of the monomeric ascorbate peroxidase that oxidizes phenol derivatives to phenoxyl radicals in presence of hydrogen peroxyde (H_2O_2)[38]. Hence APEX2 converts biotin-phenol to short-lived, small-distance diffusive biotin-phenoxyl radicals that covalently react with electron-rich amino-acid side chains. Based on biotin-phenoxyl radicals half-life and diffusion rates, it is proposed that APEX2 biotinylates macromolecules located within 20 nm radius[40]. Once fused to a bait protein, APEX2 labels proteins present within the diffusion radius, and hence proteins in contact with the bait and proteins that share the same space. These proximity-biotinylated proteins can be then enriched on streptavidin and identified by mass spectrometry. In the recent years, this approach has been successfully employed to define the mitochondrial matrix proteome, to identify partners of G-protein coupled receptors and to map the *Chlamydia trachomatis* inclusion membrane[39-46]. However, studies have been restricted to eukaryotic cells and no example of APEX2-dependent labeling is yet available inside bacterial cells. We engineered a pKD4 vector derivative, pKD4-APEX2 (Supplementary Fig. 1a), allowing insertion of the *apex2* sequence at the locus of interest on the bacterial genome using the one-step procedure[47]. The *apex2*-coding sequence was genetically fused to *tssA* (gene accession number GI:284924261), at the native chromosomal locus in the EAEC genome to generate a APEX2-TssA fusion protein (Supplementary Fig. 1b). APEX2 was fused at the N-terminus of TssA, as we previously showed that the presence of GFP at this position did not prevent T6SS activity[18]. Indeed, anti-bacterial competition assay showed that cells producing APEX2-TssA eliminate competitor *E. coli* K-12 cells at a level comparable to the wild-type strain, demonstrating that fusion of APEX2 at the N-terminus of TssA does not impact T6SS activity (Supplementary Fig. 1c). Western-blot analyses of lysates of wild-type cells producing APEX2-TssA using a streptavidin-coupled antibody showed that several proteins are specifically biotinylated in presence of biotin-phenol and H_2O_2, demonstrating that APEX2 is functional in the bacterial cytoplasm (Supplementary Fig. 1d).

Wild-type cells producing the chromosomal APEX2-TssA fusion were mixed with *E. coli* K-12 competitor cells and incubated on plates containing 10 mM biotin-phenol. This concentration of biotin-phenol does not impact bacterial growth (Supplementary Fig. 2a) nor T6SS activity (Supplementary Fig. 2b). Live cells were then treated for 1 min with H_2O_2 and biotinylated TssA proximity partners were enriched on streptavidin beads after quenching and cell lysis. The total eluate was subjected to mass spectrometry for protein identification (Table 1, first column). The highest hits correspond to T6SS subunits, including the TssM and TssL membrane proteins, the TssK, VgrG, TssF and TssG baseplate components, the Hcp and TssC tail proteins, as well as a protein of unknown function, encoded by the *EC042_4550* gene (accession number GI: 284924271; hereafter named TagA). Interestingly, TssK, VgrG, Hcp and TssC are known interacting partners of TssA[18] whereas TssF and TssG form a stable complex with TssK[24,25] and are likely at close proximity to the TssK-bound TssA. Finally, while no direct contacts have been identified between TssA and TssM and TssL, the TssA protein was previously shown to co-purify with the TssJLM complex[18]. The *EC042_4550* gene, located at close proximity to the T6SS core component genes (Supplementary Fig. 1b), encodes a protein of the TssA family, which shares the N-terminal ImpA domain but has a different C-terminal extension and was thus named TagA (Type VI accessory gene with ImpA domain)[36]. The two T6SS integral inner membrane proteins, TssM and TssL, were not retrieved when detergent was omitted during preparation of the lysate sample prior to streptavidin enrichment (Table 1, second column). No significant hits were recovered from mass spectrometry analysis of streptavidin-enriched samples from wild-type cells that do not produce APEX2-TssA (Table 1, third column). In addition, no T6SS proteins were biotinylated when APEX2 was produced from the *tssA* locus but not fused to TssA (Table 1, fourth column). Finally, we generated a EAEC strain producing a fusion between APEX2 and GspE, a cytosolic ATPase that transiently associates with the membrane-anchored Type II secretion system (T2SS)[48]. Although two known T2SS partners of GspE, GspF and GspL[49], were labeled, none of the T6SS subunit was recovered in the enriched fraction (Table 1, fifth column). All these controls experiments demonstrate the specificity of APEX2 labeling when fused to TssA.

Stage-specific blocking mutations define the temporal TssA contacts during T6SS biogenesis.

Previous data have suggested that TssA mediates sequential contacts with the membrane complex, the baseplate and the tail, during T6SS biogenesis[18,36]. We sought to test this model by arresting T6SS assembly at each stage, using non-polar mutants we previously generated. In absence of TssL, the membrane complex does not assemble and T6SS assembly is blocked at an early stage[21]. Indeed, no significant hit was recovered in a *tssL* strain (Table 2; first column). The observation that both TssM and TssL are biotinylated in *tssK* and *vgrG* cells (Table 2, second and third columns) is in agreement with the fact that the membrane complex is assembled in absence of baseplate components[25] and with the proposal that TssA is bound at the cytosolic face of the membrane complex[18,36]. Finally, the biotinylation of membrane complex and baseplate components in *hcp* cells (Table 2, fourth column) correlates with the obervation that the absence of Hcp prevents polymerization of the tail but does not impact membrane complex and baseplate assembly[25]. A schematic summary of proteins biotinylated by APEX2-TssA during T6SS biogenesis is shown in Figure 1.

TagA associates at the distal end of the sheath.

The identification of TagA, a protein of unknown function, as a proximity partner of TssA and the location of the *tagA* gene at close proximity to T6SS core component genes led us to further characterize this protein. Interestingly, TagA was not biotinylated in *tssL*, *tssK*, *vgrG* or *hcp* cells (Table 2), suggesting that it contacts TssA in the late stage (*i.e.*, tail polymerization) of T6SS biogenesis. Bacterial two-hybrid and co-immunoprecipitation assays demonstrated that TagA directly interacts with TssA (Fig. 2a and 2b). Competition assays further showed that the *tagA* mutant strain retains 12 ± 4 % of activity (Fig. 2c). Anti-bacterial activity was restored to wild-type levels upon *cis*-complementation with wild-type TagA or VSV-G-tagged TagA ($_{V}$TagA; Fig. 2c). Hence, TagA is not an essential protein for T6SS action but rather increases the efficiency of the Type VI apparatus. To gain further insights into TagA localization, we performed fractionation and fluorescence microscopy experiments. In EAEC wild-type and Δ*sci1* (*i.e.*, a strain deleted of the T6SS gene cluster, from *tssB* to *tssJ*) cells, as well as in *E. coli* K-12 (devoid of T6SS gene cluster) cells, $_{V}$TagA co-fractionnates with the EF-Tu cytoplasmic elongation factor and with membrane-associated proteins such as OmpA, TolA and TolB (Fig. 2d). However, by contrast to OmpA and TolA, $_{V}$TagA behaves similarly to the peripherally-associated membrane protein TolB: $_{V}$TagA is partly released from the membrane upon urea treatment (Fig. 2d), suggesting that TagA is a cytosolic protein that associates with the membrane independently of T6SS subunits. In

agreeement with this conclusion, fluorescence microscopy imaging of a functional TagA fusion to superfolder GFP (sfGFP-TagA; Supplementary Fig. 3) revealed that TagA assembles sub-membrane punctate foci (Fig. 3a and 3b). The association of these punctate foci with the membrane was confirmed by deconvolution analyses (Supplementary Fig. 4a). Interestingly, these foci are not randomly distributed but rather cluster at the ¼ of the cell (Fig. 3c). Time-lapse recordings in wild-type showed that these foci dynamically associate - or appear close to the ¼ and ¾ of the cell (Fig. 3d). Interestingly, the formation of static or dynamic sfGFP-TagA foci is dependent upon the T6SS subunits, as sfGFP-TagA localizes at diffuse membrane patches in Δ*sci1* cells (Supplementary Fig. 4b).

To better define the localization of TagA, we performed co-localization studies with a mCherry-tagged TssB sheath subunit. Fig. 3e shows that TagA localizes at one extremity of the sheath. Because the sheath extends from the baseplate to the opposite side of the cell, we next asked whether TagA partitions with the baseplate or locates at the distal end of the sheath. Co-localization experiments with the TssK baseplate subunit fused to the mCherry defined that sfGFP-TagA and TssK-mCherry do not co-localize, demonstrating that TagA is not a component of the baseplate (Fig. 3f and Supplementary Fig. 5). From these results, we conclude that TagA associates with the distal end of the sheath. This conclusion is in agreement with the APEX2-TssA-mediated biotinylation of TagA only in cells authorizing sheath polymerization. To gain further insights into TagA dynamics, we imaged sheath assembly in cells producing sfGFP-TagA. Examination of full cycles of sheath extension/contraction (see blue arrow in Fig. 3g) established that TagA is captured by the distal end of the sheath once it approaches the membrane (Fig. 3g, Supplementary Fig. 5, Supplementary Video 1).

TagA stops sheath polymerization and stabilizes the extended sheath conformation.

To determine the role of TagA in sheath dynamics, we imaged wild-type, *tagA* and complemented *tagA* cells producing TssB-sfGFP. Time-lapse fluorescence recordings revealed some remarkable sheath dynamics in *tagA* cells: about fifty percent of the sheaths extend toward the opposite side of the membrane but do not stop, and hence undergo a distortion event allowing their extension parallel to the membrane (Fig. 4a-b; Supplementary Video 2), ultimately leading to sheaths break or detachment from the membrane complex/baseplate (see red arrowheads in Fig. 4a). This observation suggests that in absence

of TagA, the polymerization of some of the sheaths does not stop at the opposite membrane (*i.e.*, the location of TagA) and thus that TagA may constitute the stopper – or part of the stopper – for T6SS sheath extension. These sheaths are likely to be non-productive, explaining the decreased T6SS activity in *tagA* cells. The remaining sheaths undergo usual extension/contraction cycles. However, we noticed that most of these sheaths contract rapidly after completion of their extension. Comparison of the residence time of extended sheaths (*i.e.*, duration of the extended sheath conformation prior to contraction) in wild-type, *tagA* and complemented *tagA* cells revealed that sheaths contract significantly more rapidly after tail competion in absence of TagA (Fig. 4c, Supplementary Fig. 6). Interestingly, the distribution of the residence time differs considerably between wild-type and *tagA* cells: the number of sheaths that contract immediatly after extension is significantly increased in *tagA* cells (> 60% of the events) compared to wild-type of complemented *tagA* cells (~ 5% of the events) (Fig. 4c, Supplementary Fig. 6). These results provide support to an additional role of TagA as a clamp to stabilize the extended sheath and/or to maintain the sheath under the extended conformation.

Concluding remarks

In this study we have adapted the APEX2-dependent biotin ligation technology initially developed in eukaryotic cells to study bacterial complexes. We report the identification of the *in vivo* proximity partners of the T6SS-associated TssA protein and use this approach in stage-specific blocking mutant cells to temporally resolve the TssA contacts during T6SS biogenesis. We show that TssA successively engages with different complexes: it interacts first with the inner membrane proteins of the membrane complex (TssL, TssM), and then the baseplate (TssF, TssG, TssK and VgrG,) and the tail (Hcp, TssC). This powerful approach recapitulates the known interacting partners of TssA previously identified by bacterial two-hybrid, co-precipitation and surface-plasmon resonance assays[18]. This technology also detected two known partners of the T2SS-associated GspE ATPase, GspF and GspL[49-52]. To our knowledge, this is the first report of the use of APEX2-dependent proximity biotinylation inside living bacterial cells. This approach is specifically powerful to dissect contacts of a dynamic protein that engages in different complexes during assembly of a multiprotein system or that is involved in different processes during the cell cycle. Interestingly, APEX2 fusion to TssA revealed an additional player in Type VI secretion in EAEC, TagA. TagA could not be considered as a T6SS core component as the *tagA* gene is

found associated with a limited number of T6SS gene clusters, including that of *Xenorhabdus* and *Photorhabdus* species as well as *Aeromonas hydrophila* and *Vibrio cholerae*[36]. In agreement with the phenotypes associated with the deletion of the *tagA* gene in *V. cholerae*, *VCA0121*[53], competition experiments provided evidence that TagA is not essential for T6SS activity in EAEC. However, the presence of TagA optimizes T6SS efficiency as a *tagA* mutant retains 12 ± 4 % of anti-bacterial activity compared to the wild-type strain. Domain analyses of TagA showed that it shares the N-terminal ImpA domain found in proteins of the TssA family, including EAEC TssA and *P. aeruginosa* TssA1[18,36,54], and a C-terminal extension of unknown function. These two domains are separated by a long linker comprising a stretch of hydrophobic residues predicted to be arranged as an amphipatic α-helix[36]. Indeed, TagA is a cytosolic protein that peripherally but tightly associates with the membrane. Interestingly, TagA localizes at specific positions in the cell, halfway between midcell and the cell poles. Although we do not know the cellular determinants that control this specific positioning, TagA is captured by the distal end of the sheath, likely by directly interacting with the TssA cap protein. TagA-TssA contacts might be mediated by their N-terminal ImpA domains, which have been previously shown to dimerize[18]. It is noteworthy that the *tagA* gene is usually present within T6SS gene clusters encoding TssA, but not TssA1. This observation, the interaction between the TssA and TagA, and the presence of TagA at proximity of TssA when sheath extension is completed as revealed by the *in vivo* APEX2 assay, support a functional relationship between TssA (and the distal extremity of the sheath) and TagA. Indeed, sfGFP-TagA was shown to present a diffuse membrane pattern in absence of T6SS subunits and to assemble foci at the site of contact of the distal end of the sheath with the opposite membrane. The observation that TagA is captured by the distal end of the sheath suggests a role of this accessory protein during the late stages of sheath assembly. In agreement with this suggestion, fluorescence microscopy recordings of the T6SS sheath showed two different consequences of the absence of TagA. First, aberrant sheath polymerization was observed, in which sheath polymerization does not stop at the membrane, leading to sheath distortion, bending and, ultimately, breaking. These sheaths do not contract and hence are unfruitful to destroy rival bacteria, likely explaining the decreased T6SS activity in *tagA* cells. The second consequence of the absence of TagA is the rapid contraction after sheath extension. One explanation to these two distinct events might be how the sheath hits the membrane. It has been proposed that incorporation of new Hcp hexamers in the growing tail occurs by opening the central hexaflexagon structure of TssA[18,36]. Therefore, one may hypothesize that if the sheath arrives perpendicular to the membrane, there is no room to

allow incorporation of new Hcp hexamers, hence arresting sheath polymerization. In absence of TagA, these sheaths will contract rapidly. By contrast, if the sheath does not arrive perpendicular, new Hcp hexamers can enter the TssA central lumen, allowing the sheath polymerization to proceed and causing sheath distortion and bending. One alternative hypothesis is that the absence of TagA is partly compensated by an unknown factor for preventing uncontroled sheath extension. Using the APEX2 technology to identify proteins at proximity of TagA may provide further insights into T6SS tail completion.

Based on our results, we propose that TagA associates with the cytoplasmic side of the inner membrane. Once the distal end of the sheath approaches the opposite membrane, TagA is captured, stops sheath polymerization and clamps the extended sheath to the membrane. By linking both the sheath distal extremity and the membrane, TagA prevents the immediate contraction of the sheath and maintains the tensile forces required for efficient killing. TagA is thus employed by $TssA^{+}$ T6SS as a sheath stopper and clamp.

METHODS

Bacterial strains, media and chemicals

Enteroaggregative *E. coli* was used as model micro-organism. *Escherichia coli* K-12 strains DH5α, W3110 and BTH101 were used for cloning procedures and fractionation, and bacterial two-hybrid assay, respectively. Enteroaggregative *E. coli* (EAEC) strains used in this work are isogenic derivatives of the wild-type O3:H2 17-2 strain. *E. coli* K-12 and EAEC cells were routinely grown in LB broth at 37°C, with aeration. For induction of the *sci1* T6SS gene cluster, cells were grown in Sci1-inducing medium [SIM: M9 minimal medium supplemented with glycerol (0.2%), vitamin B1 (1 $\mu g.mL^{-1}$), casaminoacids (40 $\mu g.mL^{-1}$), LB (10% v/v)][55]. Plasmids and chromosomal deletions and insertions were maintained by the addition of ampicillin (100 $\mu g.mL^{-1}$ for K-12), kanamycin (50 $\mu g.mL^{-1}$ for K-12, 50 $\mu g.mL^{-1}$ for chromosomal insertion on EAEC, 100 $\mu g.mL^{-1}$ for plasmid bearing EAEC), or chloramphenicol (40 $\mu g.mL^{-1}$). Expression of genes from pBAD or pASK-IBA vectors was induced at $A_{600\ nm} \approx 0.6$ with 0.02% of L-arabinose (Sigma-Aldrich) for 1 h or with 0.1 $\mu g.mL^{-1}$ of anhydrotetracyclin (IBA Technologies) for 45 min, respectively. For BACTH experiments, gene expression was induced by the addition of iso-propyl-β-D-thio-galactopyranoside (IPTG, Sigma-Aldrich, 0.5 mM) and plates were supplemented with 5-bromo-4-chloro-3-indolyl-β-D-galactopyranoside (X-Gal, Eurobio, 40 $\mu g.mL^{-1}$).

Strain construction

The *tagA* gene (*EC042_4550*) was deleted in the enteroaggregative *E. coli* 17-2 strain using λ-red recombination[47] as previously described[19] using plasmid pKOBEG[56]. In brief, a kanamycin cassette was amplified from plasmid pKD4 using oligonucleotides carrying 50-nucleotide extensions homologous to regions adjacent to *tagA*. After electroporation of 600 ng of column-purified PCR product, kanamycin-resistant clones were selected and verified by colony-PCR. The kanamycin cassette was then excised using plasmid pCP20[47] and confirmed by colony-PCR. The same procedure was used to introduce *APEX2* on the chromosome. The *APEX2*-coding sequence was amplified using the pKD4-Nter-APEX2 vector and inserted downstream of the start codon of the *tssA* (APEX2-TssA) or *gspE* (APEX2-GspE) genes or upstream the start codon of *tssA* (APEX2 in the T6SS gene cluster). Fluorescent reporter genes were amplified from the pKD4-Nter-sfGFP (N-terminal sfGFP fusions) or pKD4-Cter-mCherry (C-terminal mCherry fusions) vectors[18,25] and inserted on the chromosome downstream of the start codon of the *tagA* gene (sfGFP-TagA fusion) or upstream of the stop codon of the *tssK* gene (TssK-mCh fusion). For *cis*-complementation, a pKD4 derivative vector was engineered in which the *tagA* gene (or the *tagA* gene encoding an N-terminally VSV-G-tagged version of *tagA*) was placed under the control

of the *sci1* T6SS promoter. The cassette was then introduced on the chromosome of the Δ*tagA* and Δ*tagA* $tssB_{sfGFP}$ strains, at the *lacZ* locus, by λ-red recombination using pKOBEG.

Plasmid construction

PCR was performed using a Biometra thermocycler using the Q5 DNA polymerase (New England Biolabs). Enteroaggregative *E. coli* 17-2 chromosomal DNA or the pcDNA3-APEX2-NES plasmid (Addgene #49386)[38] were used as template for PCR amplification. All the plasmids have been constructed by restriction-free cloning[57]. Primers used in this study are listed in Supplementary Table 1. Briefly, the gene of interest was amplified using oligonucleotides introducing extensions annealing to the target vector. The double-stranded product of the first PCR has then been used as oligonucleotides for a second PCR using the target vector as template. PCR products were then treated with DpnI to eliminate template plasmids. All constructs have been verified by PCR and DNA sequencing (Eurofins Genomics). Plasmid pKD4-Nter-APEX2 was deposited in the Addgene plasmid repository under accession number 112868.

***In vivo* APEX2-dependent biotin labeling and identification of biotinylated proteins by mass spectrometry**

Biotin proximity labeling. Experiments were initially conducted to optimize the conditions of biotin proximity labeling, by varying the concentration of biotin phenol, the concentration of H_2O_2, and the duration of the H_2O_2 pulse. EAEC wild-type and APEX2 derivative cells were mixed with *E. coli* K-12 competitor cells and spotted on SIM plates supplemented with 10 mM biotin phenol (Biotine Tyramide; BP, Iris Biotech). After 4 h at 37°C, cells were washed with 1 mL of SIM medium to eliminate residual BP, and treated with 1 mM hydrogen peroxide (H_2O_2; Sigma Aldrich) for 1 min before quenching by washing with TSEN buffer (Tris-HCl 20 mM pH 8, sucrose 30%, EDTA 1 mM, NaCl 100 mM) supplemented with egg-white lysozyme 10 $\mu g.mL^{-1}$, 10 mM sodium ascorbate and 10 mM sodium azide. Cells were either analyzed by SDS-PAGE and Streptavidin western-blotting or lysed by resuspension in CellLytic™ B (Sigma-Aldrich) supplemented or not with 0.2% Igepal® CA-630 (Sigma-Aldrich). After 1 hour on a wheel, lysates were clarified by centrifugation at 20,000×*g* for 10 min.

Streptavidin pull-down of biotinylated proteins. The clarified cell lysate was incubated for 30 min at room temperature with 2 mg of Streptavidin-coated magnetic beads, equilibrated in CellLytic™ B buffer supplemented with Igepal CA-630. After three washes with CellLytic™ B supplemented with Igepal CA-630, the beads were resuspended in Laemmli loading dye and loaded on a SDS-PAGE gel. The migration was stopped when the sample reached the interface between concentrating and separating gels, and the band containing the total biotinylated proteins was cut out.

Mass spectrometry analyses. The protein-containing SDS-PAGE gel bands were washed with 100 mM acetonitrile/ammonium bicarbonate pH 7.5, reduced by 10 mM dithiothreitol in 100 mM ammonium bicarbonate pH 7.5, alkylated by 55 mM iodoacetamide in 100 mM ammonium bicarbonate pH 7.5, and overnight digested at 37 °C by Trypsin/Lys-C Mix from *Pseudomonas aeruginosa* (Promega) at 10 $ng.\mu L^{-1}$ in 25 mM ammonium bicarbonate pH 7.5/proteaseMAX™ surfactant 0.025% (v/v). Tryptic peptides were extracted from gels by 0.1% (vol/vol) trifluoroacetic acid (TFA)/0.01% (vol/vol) proteaseMAX™/50% (vol/vol) acetonitrile, and dried by speed vacuum. Solubilized samples in 0.05% (vol/vol) TFA /2 % (vol/vol) acetonitrile were analyzed on a ESI-Q-Exactive Plus (ThermoFisher) mass spectrometer coupled to a nanoliquid chromatography (Ultimate 3000, Dionex). Peptides were eluted from a C18 column (Acclaim PepMap RSLC, 75 µm × 150 mm, 2 µm, 100 Å, Dionex) by a 6-40% linear gradient of mobile phase B (0.1% (vol/vol) formic acid (FA)/80% (vol/vol) acetonitrile) in mobile phase A (0.1% (vol/vol) FA) for 52 min. The peptides were detected in the mass spectrometer in a positive ion mode using a Top 10 Data Dependent workflow. One scan event full MS in the Orbitrap at 70,000, in a 350-1900 m/z range was followed by a fragmentation MS/MS step, at 17,500, of the 10 top ions, in the Higher Energy Collisional Dissociation cell set at 27. The spectra were processed by Proteome Discoverer software (ThermoFisher, version: 2.1.0.81) using the Sequest HT algorithm with the search following parameters: enteroaggregative *E. coli* 042 database (Taxonomy ID 216592 downloaded from NCBI by Protein Center, 4921 entries); trypsin enzyme (maximum 2 missed cleavages); fixed modification: carbamidomethyl (Cys); variable modification: oxidation (Met); mass values specific for monoisotopic; precursor mass tolerance: ± 10 ppm; fragment mass tolerance: ± 0.02 Da. Peptide validation was based on the best Peptide Spectrum Match (PSM) defined at a 0.05 maximum Delta Cn and a 0.01 Strict Target False Discovery Rate. Proteins were identified if minimum 2 unique peptide sequences more than 6 amino-acids passed the high confidence filter. Human keratin being considered as a common contaminant in protein identification by mass spectrometry, only hits with a number of PSM higher than keratin were considered significant. Mass spectrometry datasheets are available in Supplementary Datasheets 1-9. The experiments were done in triplicate and a representative result is shown.

Cell fractionation

Cell fractionation assay was performed as previously described[15,23,25]. Briefly, 5×10^{10} exponentially growing cells were resuspended in 750 µl of TSEN buffer and incubated for 10 min on ice. After addition of 100 $\mu g.mL^{-1}$

of lysozyme and further incubation for 20 min on ice, 750 µL of TN buffer (Tris-HCl 10 mM, pH 8.0, NaCl 100 mM) was added, and cells were lysed by three cycles of freezing and thawing and four cycles of sonication. Unbroken cells were removed by centrifugation, and soluble and membrane fractions were separated by ultracentrifugation for 45 min at 45,000×*g*. Membranes were washed once with TE buffer and resuspended in 1 mL of TN buffer supplemented with 8 M urea, incubated on a wheel for 1 h at 25°C, and then centrifuged for 45 min at 45,000×*g* to separate integral membrane and peripherally membrane associated proteins. Soluble and membrane-associated fractions were resuspended in loading buffer and subjected to SDS-PAGE and immunoblotting. Anti-EF-Tu (HyCult Biotech, clone mAb900), anti-VSV-G (Sigma-Aldrich, clone P5D4), anti-OmpA, anti-TolA and anti-TolB (laboratory collection) antibodies were used to identify the cytoplasmic Tu elongation factor, the VSV-G-tagged TagA protein, the outer membrane OmpA protein, the inner membrane TolA protein, and the outer membrane-peripherally-associated periplasmic TolB protein, respectively. The experiments were done in triplicate and a representative result is shown.

Bacterial two-hybrid assay (BACTH)

The adenylate cyclase-based bacterial two-hybrid technique[58] was used as previously published[59]. Briefly, the proteins to be tested were fused to the isolated T18 and T25 catalytic domains of the *Bordetella* adenylate cyclase. After introduction of the two plasmids producing the fusion proteins into the BTH101 reporter strain, plates were incubated at 30°C for 24 h. Three independent colonies for each transformation were inoculated into 600 µL of LB medium supplemented with ampicillin, kanamycin, and IPTG (0.5 mM). After overnight growth at 30°C, 10 µL of each culture was spotted onto LB plates supplemented with ampicillin, kanamycin, IPTG, and X-gal and incubated at 30°C. Controls include interaction assays with TolB and Pal, two protein partners unrelated to the T6SS. The experiments were done in triplicate and a representative result is shown.

Co-immuno-precipitation

Soluble lysates from 2×10^{10} cells producing VSV-G-tagged TagA or VSV-G-tagged TagA and FLAG-tagged TssA were obtained using the cell fractionation procedure, and subjected to immuno-precipitation on anti-FLAG M2 affinity gel (Sigma-Aldrich) for 1 h at 20°C. Beads were washed three times with TN buffer, resuspended in non-reducing Laemmli loading dye, and subjected to SDS-PAGE and immuno-blot analyses using monoclonal anti-VSV-G (Sigma-Aldrich, clone P5D4) and anti-FLAG (Sigma-Aldrich, clone M2) antibodies. The experiments were done in triplicate and a representative result is shown.

Inter-bacterial competition

The anti-bacterial growth competition assay was performed as described[60]. The WT *E. coli* strain W3110 bearing the kanamycin resistant pUA66-*rrnB* plasmid[61] was used as prey in the competition assay. The pUA66-*rrnB* plasmid provides a strong constitutive green fluorescent (GFP^+) phenotype. Attacker and prey cells were grown in SIM medium to a $A_{600nm} \approx 0.6$-0.8, harvested and normalized to a A_{600nm} of 10 in SIM. Attacker and prey cells were mixed to a 4:1 ratio and 15-µL drops of the mixture were spotted in triplicate onto a prewarmed dry SIM agar plate. After 4-hour incubation at 37°C, fluorescent images were recorded with a LI-COR Odyssey imager. The bacterial spots were scratched off, and cells were resuspended in LB medium and normalized to a A_{600nm} of 0.5. For fluorescence measurements, triplicates of 200 µl were transferred into wells of a black 96-well plate (Greiner) and the A_{600nm} and fluorescence (excitation: 485 nm; emission: 530 nm) were measured with a TECAN infinite M200 microplate reader (9 measures per mixture per experiment). The relative fluorescence was expressed as the intensity of fluorescence divided by the A_{600nm}, after subtracting the values of a blank sample. For enumeration of viable *E. coli* K-12 cells, serial dilutions were plated on kanamycin plates and the number of colonies were counted after 16-h incubation at 37°C. The experiments were done in triplicate and a representative result is shown. Statistical analyses of inter-bacterial competition assays were performed by Student's *t*-test. Significant differences were defined as $p < 0.05$ (*), $p < 0.01$ (**), and $p < 0.001$ (***).

Fluorescence microscopy.

Cells were grown in SIM to a $A_{600\ nm} \approx 0.4$–0.6, harvested and resuspended in fresh SIM to a $A_{600\ nm} \approx 10$. Cell mixtures were spotted on a thin pad of SIM supplemented with 2% agarose, covered with a cover slip and incubated for 20-30 min at room temperature before microscopy acquisition. Fluorescence microscopy was performed with a Nikon Eclipse Ti microscope equipped with an Orcaflash 4.0 LT digital camera (Hamamatsu) and a perfect focus system (PFS) to automatically maintain focus so that the point of interest within a specimen is always kept in sharp focus at all times despite mechanical or thermal perturbations. All fluorescence images were acquired with a minimal exposure time to minimize bleaching and phototoxicity effects. Exposure times were typically 20 ms for phase contrast, 100 ms for TssB-GFP, 2000 ms for sfGFP-TagA and 800 ms for TssB-mCherry and TssK-mCherry. The experiments were done in triplicate and a representative result is shown. For fluorescence microscopy, statistical analyses were performed using several representative fields from three independent biological replicates. Images were analyzed using ImageJ (http://imagej.nih.gov/ij/) and the

MicrobeJ plugin (http://www.microbej.com/)[62] or Zen (Carl Zeiss). Statistical dataset analysis was performed using Excel and the R software environment (https://www.r-project.org/). Contractile sheath residence time was determined as the number of frames during which the sheath remained fully extended. Only sheaths that performed visible extension and contraction within the movie period were considered.

Data availability.

Excel sheets with the raw mass-spectrometry data are provided as Supplementary Datasheets 1-9. Plasmid pKD4-Nter-APEX2 has been deposited in the Addgene plasmid repository under accession number 112868. All data that support the findings of this study are available from the corresponding author upon request.

References

1. Basler, M., Pilhofer, M., Henderson, G.P., Jensen, G.J., & Mekalanos, J.J. Type VI secretion requires a dynamic contractile phage tail-like structure. *Nature* **483**, 182–186. (2012).

2. Brunet, Y.R., Espinosa, L., Harchouni, S., Mignot, T., & Cascales, E. Imaging type VI secretion-mediated bacterial killing. *Cell Rep.* **3**, 36–41. (2013).

3. Basler, M. Type VI secretion system: secretion by a contractile nanomachine. *Philos Trans R Soc Lond B Biol Sci* **370**, 1679. (2015).

4. Zoued, A., *et al.* Architecture and assembly of the Type VI secretion system. *Biochim Biophys Acta* **1843**, 1664–1673. (2014).

5. Durand, E., Cambillau, C., Cascales, E., & Journet, L. VgrG, Tae, Tle, and beyond: the versatile arsenal of Type VI secretion effectors. *Trends Microbiol.* **22**, 498–507. (2014).

6. Ho, B.T., Dong, T.G., & Mekalanos, J.J. A view to a kill: the bacterial type VI secretion system. *Cell Host Microbe* **15**, 9–21. (2014).

7. Cianfanelli, F.R., Monlezun, L., & Coulthurst, S.J. Aim, load, fire: the type VI secretion system, a bacterial nanoweapon. *Trends Microbiol* **24**, 51–62. (2016).

8. Brackmann, M., Nazarov, S., Wang, J., & Basler, M. Using force to punch holes: mechanics of contractile nanomachines. *Trends Cell Biol* **27**, 623–632. (2017).

9. Russell, A.B., Peterson, S.B., & Mougous, J.D. Type VI secretion system effectors: poisons with a purpose. *Nat Rev Microbiol* **12**, 137–148. (2014).

10. Alcoforado Diniz, J., Liu, Y.C., & Coulthurst, S.J. Molecular weaponry: diverse effectors delivered by the Type VI secretion system. *Cell Microbiol* **17**, 1742–1751. (2015).

11. Chassaing, B., & Cascales, E. Antibacterial weapons: targeted destruction in the microbiota. *Trends Microbiol.* **26**, 329-338 (2018).

12. Hachani, A., Wood, T.E., & Filloux, A. Type VI secretion and anti-host effectors. *Curr Opin Microbiol.* **29,** 81-93 (2016).

13. Ryu, C.M. Against friend and foe: type 6 effectors in plant-associated bacteria. *J Microbiol.* **53,** 201-8 (2015).

14. Si, M., *et al*. The type VI secretion system engages a redox-regulated dual-functional heme transporter for zinc acquisition. *Cell Rep.* **20,** 949-959 (2017).

15. Aschtgen, M.S., Gavioli, M., Dessen, A., Lloubès, R., & Cascales, E. The SciZ protein anchors the enteroaggregative *Escherichia coli* Type VI secretion system to the cell wall. *Mol Microbiol* **75**, 886–899. (2010).

16. Shneider, M.M., *et al*. PAAR-repeat proteins sharpen and diversify the type VI secretion system spike. *Nature* **500**, 350–353. (2013).

17. Weber, B.S., *et al*. Genetic dissection of the type VI secretion system in *Acinetobacter* and identification of a novel peptidoglycan hydrolase, TagX, required for its biogenesis. *MBio* **7**, pii: e01253-16. (2016).

18. Zoued, A., *et al*. Priming and polymerization of a bacterial contractile tail structure. *Nature* **531**, 59–63. (2016).

19. Aschtgen, M.S., Bernard, C.S., de Bentzmann, S., Lloubès, R., and Cascales, E. SciN is an outer membrane lipoprotein required for type VI secretion in enteroaggregative *Escherichia coli*. *J Bacteriol* **190**, 7523–7531. (2008).

20. Felisberto-Rodrigues, C., *et al*. Towards a structural comprehension of bacterial type VI secretion systems: characterization of the TssJ-TssM complex of an *Escherichia coli* pathovar. *PLoS Pathog* **7**, e1002386. (2011).

21. Durand, E., *et al*. Biogenesis and structure of a type VI secretion membrane core complex. *Nature* **523**, 555–560. (2015).

22. Santin, Y.G., & Cascales, E. Domestication of a housekeeping transglycosylase for assembly of a Type VI secretion system. *EMBO Rep* **18**, 138–149. (2017).

23. Zoued, A., *et al*. TssK is a trimeric cytoplasmic protein interacting with components of both phage-like and membrane anchoring complexes of the type VI secretion system. *J Biol Chem* **288**, 27031–27041. (2013).

24. English, G., Byron, O., Cianfanelli, F.R., Prescott, A.R., & Coulthurst, S.J. Biochemical analysis of TssK, a core component of the bacterial Type VI secretion system, reveals distinct oligomeric states of TssK and identifies a TssK-TssFG subcomplex. *Biochem J* **461**, 291–304. (2014).

25. Brunet, Y.R., Zoued, A., Boyer, F., Douzi, B., & Cascales, E. The type VI secretion TssEFGK-VgrG phage-like baseplate is recruited to the TssJLM membrane complex via multiple contacts and serves as assembly platform for tail tube/sheath polymerization. *PLoS Genet* **11**, e1005545. (2015).

26. Taylor, N.M., *et al*. Structure of the T4 baseplate and its function in triggering sheath contraction. *Nature* **533**, 346–352. (2016).

27. Leiman, P.G., *et al*. Type VI secretion apparatus and phage tail-associated protein complexes share a common evolutionary origin. *Proc Natl Acad Sci U S A* **106**, 4154–4159. (2009).

28. Büttner, C.R., Wu, Y., Maxwell, K.L., & Davidson, A.R. Baseplate assembly of phage Mu: defining the conserved core components of contractile-tailed phages and related bacterial systems. *Proc Natl Acad Sci U S A* **113**, 10174–10179. (2016).

29. Nguyen, V.S., *et al*. Type VI secretion TssK baseplate protein exhibits structural similarity with phage receptor-binding proteins and evolved to bind the membrane complex. *Nat Microbiol* **2**, 17103. (2017).

30. Nazarov, S., Schneider, J.P., Brackmann, M., Goldie, K.N., Stahlberg, H., & Basler, M. Cryo-EM reconstruction of Type VI secretion system baseplate and sheath distal end. *EMBO J.* in press (pii: e201797103). (2018).

31. Logger, L., Aschtgen, M.S., Guérin, M., Cascales, E., & Durand, E. Molecular dissection of the interface between the type VI secretion TssM cytoplasmic domain and the TssG baseplate component. *J Mol Biol* **428**, 4424–4437. (2016).

32. Zoued, A., *et al*. Structure-function analysis of the TssL cytoplasmic domain reveals a new interaction between the type VI secretion baseplate and membrane complexes. *J Mol Biol* **428**, 4413–4423. (2016).

33. Brunet, Y.R., Hénin, J., Celia, H., & Cascales, E. Type VI secretion and bacteriophage tail tubes share a common assembly pathway. *EMBO Rep* **15**, 315–321. (2014).

34. Kudryashev, M., *et al*. Structure of the type VI secretion system contractile sheath. *Cell* **160**, 952–962. (2015).

35. Wang, J., *et al*. Cryo-EM structure of the extended type VI secretion system sheath-tube complex. *Nat Microbiol* **2**, 1507–1512. (2017).

36. Zoued, A., *et al*. TssA: the cap protein of the Type VI secretion tail. *Bioessays* **39**, 00262. (2017).

37. Vettiger, A., Winter, J., Lin, L., & Basler, M. The type VI secretion system sheath assembles at the end distal from the membrane anchor. *Nat Commun* **8**, 16088. (2017).

38. Lam, S.S., *et al*. Directed evolution of APEX2 for electron microscopy and proximity labeling. *Nat Methods* **12**, 51–54. (2015).

39. Lobingier, B.T., *et al*. An approach to spatiotemporally resolve protein interaction networks in living cells. *Cell* **169**, 350–360. (2017).

40. Rhee, H.W., *et al*. Proteomic mapping of mitochondria in living cells via spatially restricted enzymatic tagging. *Science* **339**, 1328–1331. (2013).

41. Hung, V., *et al*. Proteomic mapping of the human mitochondrial intermembrane space in live cells via ratiometric APEX tagging. *Mol Cell* **55**, 332–341. (2014).

42. Hung, V., *et al*. Spatially resolved proteomic mapping in living cells with the engineered peroxidase APEX2. *Nat Protoc* **11**, 456–475. (2016).

43. Lee, S.Y., Kang, M.G., Park, J.S., Lee, G., Ting, A.Y., & Rhee, H.W. APEX fingerprinting reveals the subcellular localization of proteins of interest. *Cell Rep* **15**, 1837–1847. (2016).

44. Hung, V., *et al*. Proteomic mapping of cytosol-facing outer mitochondrial and ER membranes in living human cells by proximity biotinylation. *Elife* **6**, e24463. (2017).

45. Paek, J., *et al*. Multidimensional tracking of GPCR signaling via peroxidase-catalyzed proximity labeling. *Cell* **169**, 338–349. (2017).

46. Rucks, E.A., Olson, M.G., Jorgenson, L.M., Srinivasan, R.R., & Ouellette, S.P. Development of a proximity labeling system to map the *Chlamydia trachomatis* inclusion membrane. *Front Cell Infect Microbiol* **7**, 40. (2017).

47. Datsenko, K.A., & Wanner, B.L. One-step inactivation of chromosomal genes in *Escherichia coli* K-12 using PCR products. *Proc Natl Acad Sci U S A* **97**, 6640–6645. (2000).

48. Chen, Y.L., & Hu, N.T. Function-related positioning of the type II secretion ATPase of *Xanthomonas campestris* pv. *campestris*. *PLoS One* **8**, e59123. (2013).

49. Py, B., Loiseau, L., & Barras F. An inner membrane platform in the type II secretion machinery of Gram-negative bacteria. *EMBO Rep* **2**, 244–248. (2001).

50. Py, B., Loiseau, L., & Barras, F. Assembly of the type II secretion machinery of *Erwinia chrysanthemi*: direct interaction and associated conformational change between OutE, the putative ATP-binding component and the membrane protein OutL. *J Mol Biol* **289**, 659–670. (1999).

51. Abendroth, J., Murphy, P., Sandkvist, M., Bagdasarian, M., & Hol, W.G. The X-ray structure of the type II secretion system complex formed by the N-terminal domain of EpsE and the cytoplasmic domain of EpsL of *Vibrio cholerae. J Mol Biol* **348**, 845–855. (2005).

52. Arts, J., *et al*. Interaction domains in the *Pseudomonas aeruginosa* type II secretory apparatus component XcpS (GspF). *Microbiology* **153**, 1582–1592. (2007).

53. Zheng, J., Ho, B., & Mekalanos, J.J. Genetic analysis of anti-amoebae and anti-bacterial activities of the type VI secretion system in *Vibrio cholerae. PLoS One* **6**, e23876. (2011).

54. Planamente, S., Salih, O., Manoli, E., Albesa-Jové, D., Freemont, P.S., & Filloux, A. TssA forms a gp6-like ring attached to the type VI secretion sheath. *EMBO J* **35**, 1613–1627. (2016).

55. Brunet, Y.R., Bernard, C.S., Gavioli, M., Lloubès, R., & Cascales, E. An epigenetic switch involving overlapping fur and DNA methylation optimizes expression of a type VI secretion gene cluster. *PLoS Genet* **7**, e1002205. (2011).

56. Chaveroche, M.-K., Ghigo, J.-M., & d' Enfert, C. A rapid method for efficient gene replacement in the filamentous fungus *Aspergillus nidulans*. *Nucleic Acids Res* **28**, e97. (2000).

57. van den Ent, F., & Löwe, J. RF cloning: a restriction-free method for inserting target genes into plasmids. J. *Biochem. Biophys. Methods* **67**, 67–74. (2006).

58. Karimova, G., Pidoux, J., Ullmann, A., & Ladant, D. A bacterial two-hybrid system based on a reconstituted signal transduction pathway. *Proc Natl Acad Sci U S A* **95**, 5752–5756. (1998).

59. Battesti, A., & Bouveret, E. The bacterial two-hybrid system based on adenylate cyclase reconstitution in *Escherichia coli*. *Methods* **58**, 325–334. (2012).

60. Flaugnatti, N., et al. A phospholipase A1 antibacterial Type VI secretion effector interacts directly with the C-terminal domain of the VgrG spike protein for delivery. *Molecular Microbiology* **99**, 1099–1118. (2016).

61. Zaslaver, A., *et al*. A comprehensive library of fluorescent transcriptional reporters for *Escherichia coli*. *Nat. Methods* **3**, 623–628. (2006).

62. Ducret, A., Quardokus, E.M., & Brun, Y.V. MicrobeJ, a tool for high throughput bacterial cell detection and quantitative analysis. *Nat Microbiol* **1**, 16077. (2016).

Correspondence and requests for materials should be addressed to E.C. (cascales@imm.cnrs.fr).

Acknowledgments

This work was funded by the Centre National de la Recherche Scientifique, the Aix-Marseille Université, and grants from the Agence Nationale de la Recherche (ANR-14-CE14-0006-02, ANR-17-CE11-0039-01). Y.G.S. is supported by a doctoral fellowship from the French ministry of research. We thank Hugo Le Guenno of the IMM microscopy facility for helpful advices regarding deconvolution analyses, James Sturgis (IMM, Marseille), Elizabeth (Lisa) A. Rucks and Scott Ouellette (University of South Dakota, Vermillion, USA) for initial discussions on biotin-dependent ligation; the members of the Cascales, Lloubès, Sturgis and Bouveret research groups for discussions; M. Ba, I. Bringer, A. Brun and O. Uderso for technical assistance, and the three anonymous reviewers for their constructive comments.

Authors Contributions

Y.G.S. & E.C. designed and conceived the experiments. Y.G.S., T.D., R.L., L.E. performed the experiments. Y.G.S. performed all the experiments, with the help of T.D. and L.E. for fluorescence

590 microscopy. R.L. performed the mass spectrometry analyses. E.C supervised the execution of the
591 experiments. L.J. & E.C. provided tools. E.C. wrote the paper with contributions of Y.G.S, T.D., R.L.
592 and L.J.

593 ## Additional Information

594 **Supplementary Information** is available for this manuscript. It includes one Supplementary Table,
595 seven Supplementary Figures, two Supplementary Videos, and nine Supplementary Datasheets.

596

597 **Competing Interests**
598 The authors declare no competing financial interests.

599

Legend to Figures

Figure 1 | Summary of TssA proximity partners. The different stages of T6SS assembly are depicted (1, assembly of the membrane complex; 2, baseplate recruitment and docking; 3, polymerization of the tail), as well as the stage-blocking mutations used in this study (deletion of the *tssK* or *vgrG* gene stops T6SS assembly at stage 1 whereas deletion of the *hcp* gene stops T6SS assembly at stage 2). The TssA protein is shown in red and the other T6SS subunits are indicated (J corresponds to TssJ). The blue color highlights the subunits that are biotinylated by the functional APEX2-TssA fusion protein.

Figure 2 | TagA is an accessory T6SS cytosolic component that associates with the membrane. a and **b,** TagA interacts directly with TssA. **a,** BACTH assay. BTH101 reporter cells producing the indicated proteins fused to the T18 and T25 domain of the *Bordetella* adenylate cyclase were spotted on X-Gal-IPTG reporter LB agar plates. The BACTH experiment was performed in triplicate with identical results. **b,** Co-immunoprecipitation assay. Soluble lysates of *E. coli* cells producing VSV-G-tagged TagA ($_{V}$TagA) alone or $_{V}$TagA with FLAG-tagged TssA (TssA$_{F}$) were subjected to immunoprecipitation with anti-FLAG-coupled beads. The total lysates (T) and immunoprecipitated (IP) material were separated by 12.5% acrylamide SDS-PAGE and immunodetected with anti-FLAG (upper panel) and anti-VSV-G (lower panel) monoclonal antibodies. Molecular weight markers (in kDa) are indicated on left. The co-immunoprecipitation experiment was performed in triplicate with identical results. **c,** TagA optimizes T6SS activity. Antibacterial competition assay. *E. coli* K-12 competitor cells (W3110 *gfp*$^{+}$, kan^{R}) were mixed with the indicated attacker cells, spotted onto SIM agar plates, and incubated for 4 h at 37 °C. The fluorescence of the bacterial spot (in arbitrary units, bars represent the average, standard deviation are indicated, dot plots (grey circles) are overlaid) is shown on top. The number of surviving *E. coli* competitor cells (counted on selective kanamycin medium) is indicated in the lower graph (in $\log_{10}$ of colony forming units). The circles indicate the values from three independent assays, and the average is indicated by the bar. Statistical significance relative to the wild-type strain is indicated (*p*-values; NS, non significant; *, $p < 0.05$; **, $p < 0.01$, two-sided Student's *t*-test; *p*-values for fluorescence measurements (upper graph): Δ*tssA*, 0.000196; Δ*tagA*, 0.0086; $_{V}$*tagA*$^{+}$, 0.119; *tagA*$^{+}$, 0.746; *p*-values for *E. coli* K-12 survival (lower graph): Δ*tssA*, 0.00219; Δ*tagA*, 0.0194; $_{V}$*tagA*$^{+}$, 0.531; *tagA*$^{+}$, 0.831). **d,** TagA fractionates with soluble and peripherally-associated membrane proteins. Fractionation assay.

Total extracts (T) of WT or Δ*sci1* EAEC, or *E. coli* K-12 cells producing $_{V}$TagA were subjected to fractionation to separate the soluble (S) and membrane (M) fractions. Peripherally-associated (pM) and integral (iM) membrane proteins were separated by treatment with 8 M urea. Control markers include the integral outer membrane OmpA protein, the integral inner membrane TolA protein, the peripherally-associated membrane TolB protein, and the EF-Tu cytoplasmic elongation factor. Molecular weight markers (in kDa) are indicated on left. Fractionation experiments were performed in triplicate with identical results. Uncropped blots are shown in Supplementary Fig. 7.

Figure 3 | TagA localizes at the cell quarters and binds the distal end of the sheath. a, Fluorescence microscopy recording of wild-type EAEC cells producing sfGFP-TagA (upper panel, phase channel; lower panel, GFP channel). Localization of TagA clusters are indicated by white arrowheads. Scale bar, 1 μm. Fluorescence microscopy recordings have been performed thirty times with identical results. A deconvolution analysis of WT EAEC cells producing sfGFP-TagA is shown in Supplementary Fig. 4a. **b,** Number of sfGFP-TagA foci per cell. The percentage of cells with 0, 1, 2 or >2 foci is indicated (*n*= 1171 cells from three biological replicates, bars represent the average, standard deviation are indicated, dot plots (grey circles) are overlaid). The mean number of foci per cell is 0.74 ± 0.24. **c,** Spatial repartition of sfGFP-TagA foci. Shown is a projection of the foci from *n* = 316 cells on a single cell (from blue (low abundance) to yellow (high abundance)). **d,** Fluorescence microscopy time-lapse recording of EAEC cells producing sfGFP-TagA. Individual images were taken every 40 s. The localization of TagA is indicated by the white arrowhead. A schematic diagram representating the dynamics of TagA is shown below. Scale bar, 1 μm. Time-lapse recordings have been performed thirty times with identical results. A statistical analyses of the distribution of sfGFP-TagA dynamics in wild-type and Δ*sci1* cells is shown in Supplementary Fig. 4b. **e** and **f,** Co-localization of sfGFP-TagA with TssB-mCherry (**e**) or TssK-mCherry (**f**). From top to bottom are shown the GFP, and mCherry channels, an overlay of the GFP and mCherry channels and a schematic representation. Scale bar, 1 μm. Statistical analyses of TagA co-localization with TssK and TssB are shown in Supplementary Figure 5. Co-localization recordings have been performed three and five times for TssK-mCherry and TssB-mCherry, respectively, with identical results. **g**, Fluorescence microscopy time-lapse recording of EAEC cells producing sfGFP-TagA and TssB-mCherry. Individual images were taken every 30 s. White arrowheads indicate assembly or contraction events whereas the blue arrowheads point at a complete assembly-contraction cycle. A schematic diagram

representating a complete cycle is shown below. Scale bar, 1 μm. See also Supplementary Video 1. Statistical analyses of co-localization of sfGFP-TagA with TssK-mCherry or with the distal end of the sheath are shown in Supplementary Fig. 5. Time-lipse co-localization recordings have been performed five times with identical results.

Figure 4 | TagA stops sheath elongation and maintains the sheath under the extended conformation. a, Sheath dynamics. Fluorescence microscopy time-lapse recording of EAEC wild-type (WT), Δ*tagA* cells or Δ*tagA* cells expressing *tagA* (Δ*tagA* *tagA*$^+$), producing TssB-sfGFP. Individual images were taken every 40 s. White arrowheads indicate complete assembly-contraction cycles whereas blue arrowheads indicate sheaths that do not stop at the opposite membrane and bend. Red arrowheads point sheath detachment from the membrane complex/baseplate. Scale bar, 1 μm. See also Supplementary Video 2. Time-lapse recordings have been performed in triplicate with identical results. **b,** Quantification of the different sheath assembly events (blue, sheaths that stop at the opposite membrane; green, sheaths that do not stop at the opposite membrane, bend and break). The number of sheath events analyzed for each strain (*n*) is indicated on top, standard deviation are indicated by the vertical bar, dot plots (grey circles) are overlaid. **c,** Violin plot representation of the sheath residence time. The distribution of the sheath residence time in wild-type (WT, blue), Δ*tagA* (red) cells and Δ*tagA* expressing *tagA* (Δ*tagA* *tagA*$^+$, green) is represented as a violin plot. The bold horizontal bar represents the median values; the closed circle represents the mean: the lower and upper boundaries of the internal box plot correspond to the 25% and 75% percentiles respectively; the whiskers represent the 10% and 90% percentiles. Outliers are shown as black stars. The distribution is indicated by the outer shape. The number of sheath assembly/contraction events (*n*) is indicated on right, as well as the mean and the standard deviation, and the statistical significance relative to WT (NS, non significative; ****, $p < 0.0001$; two-sided Wilcoxon's *t*-test; *p*-values: Δ*tagA*, 2.2×10^{-16}; *tagA*$^+$, 0.62). The distribution is shown as a graph in Supplementary Fig. 6.

Table 1. Mass spectrometry identification of proteins after APEX2-dependent proximity biotinylation.

The highest ranked proteins are indicated, as well as the number of Peptide Spectral Matches (PSM), *i.e.*, the number of validated peptides for the corresponding protein, indicating its relative abundance. The mass spectrometry datasheets are available in supplemental data files.

APEX-TssA[a]		APEX-TssA[a,b]		none[c]	APEX[d]		APEX-GspE[e]	
TssM	760	VgrG	405		AceF	120	GspL	377
TssK	311	TssK	365				GspF	323
VgrG	306	Hcp	349					
Hcp	258	TagA	234					
TssF	211	TssF	222					
TagA	193	TssC	87					
TssL	163	TssG	89					
TssG	64*							
TssC	54*							

[a] *apex2* fused at the 5' of *tssA*.
[b] no detergent used in the preparation of cell lysate.
[c] no *apex2* inserted on the chromosome.
[d] *apex2* inserted in the T6SS gene cluster.
[e] *apex2* fused at the 5' of *gspE*.
* T6SS proteins with lower abundance than human keratin

Table 2. Mass spectrometry identification of proteins after APEX2-dependent proximity biotinylation in stage-blocking mutant cells.

The highest ranked proteins are indicated, as well as the number of Peptide Spectral Matches (PSM), *i.e.*, the number of validated peptides for the corresponding protein, indicating its relative abundance. The mass spectrometry datasheets are available in supplemental data files.

Δ*tssL*		Δ*tssK*		Δ*vgrG*		Δ*hcp*	
AceF	39	TssM	893	TssM	1343	TssM	1173
		TssL	222	TssL	296	TssK	460
		AceF	76	AceF	67	VgrG	448
						TssF	241
						TssL	235
						TssG	102

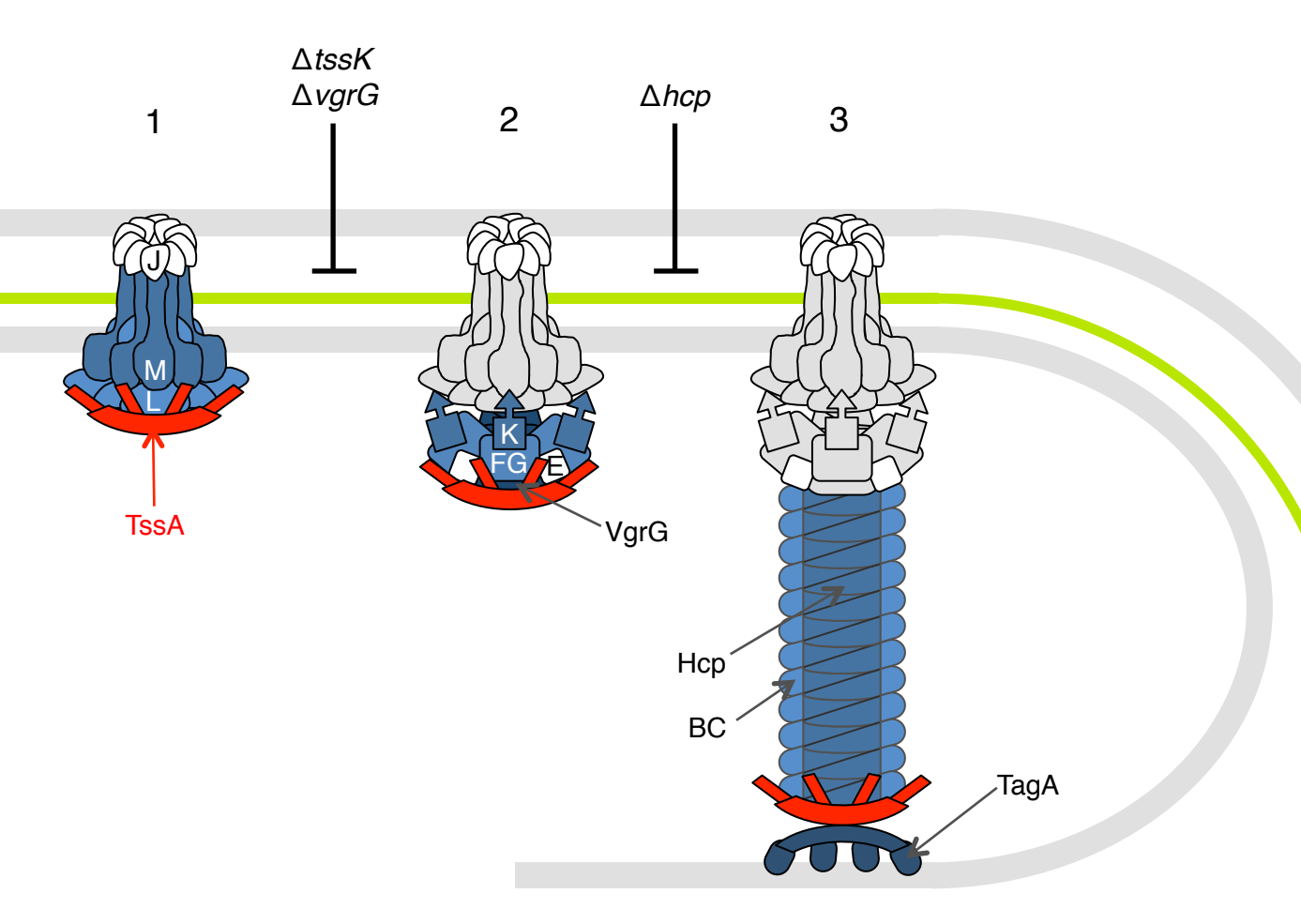
1
ΔtssK
ΔvgrG
2
Δhcp
3
J
M
L
TssA
K
FG
E
VgrG
Hcp
BC
TagA

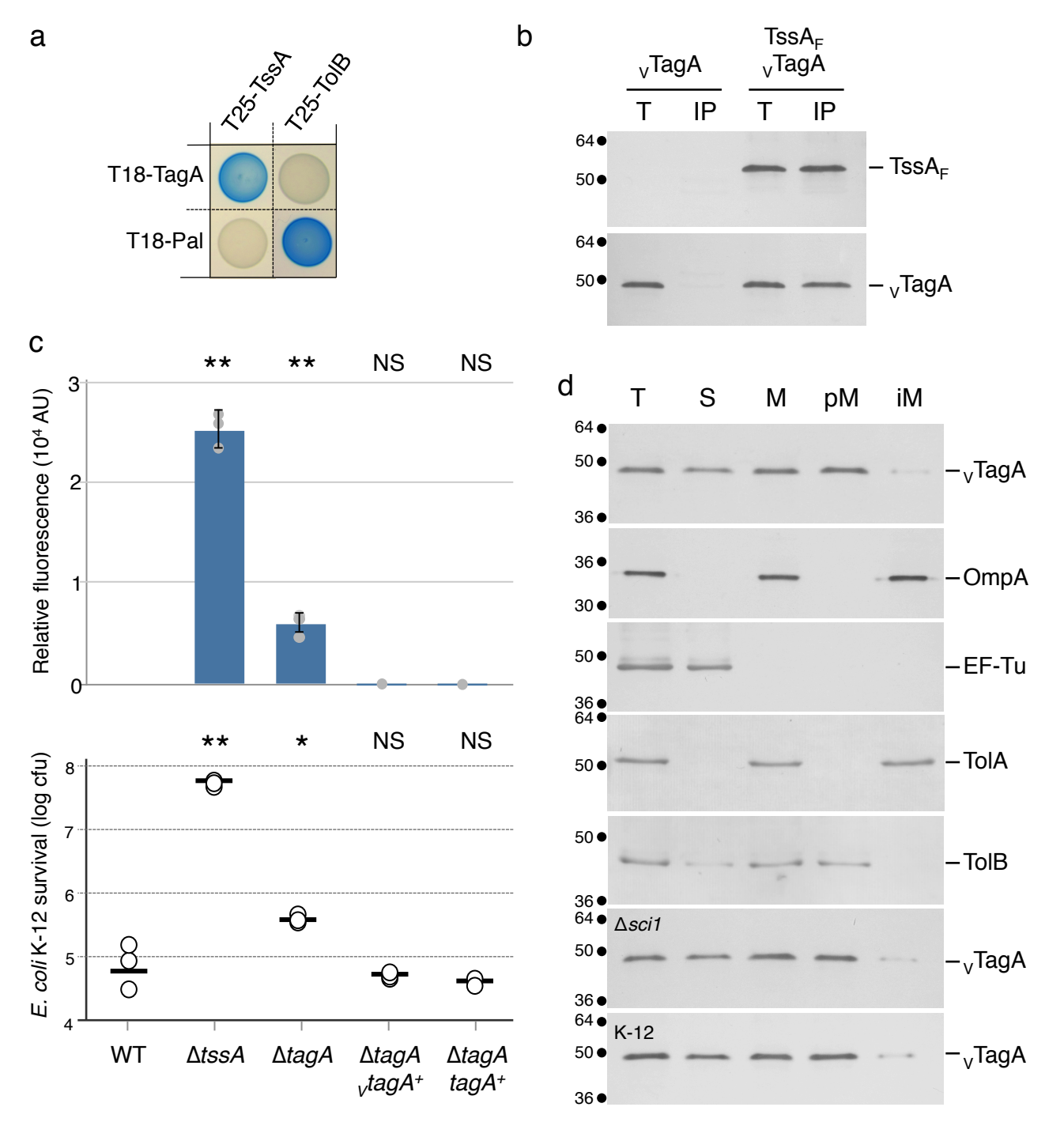
a
T25-TssA
T25-TolB
T18-TagA
T18-Pal
b
VTagA
TssAF VTagA
T
IP
T
IP
64
50
TssAF
64
50
VTagA
c
**
**
NS
NS
Relative fluorescence (10⁴ AU)
3
2
1
0
**
*
NS
NS
E. coli K-12 survival (log cfu)
8
7
6
5
4
WT
ΔtssA
ΔtagA
ΔtagA VtagA+
ΔtagA tagA+
d
T
S
M
pM
iM
64
50
36
VTagA
36
30
OmpA
50
36
EF-Tu
64
50
TolA
50
36
TolB
64
Δsci1
50
36
VTagA
64
K-12
50
36
VTagA

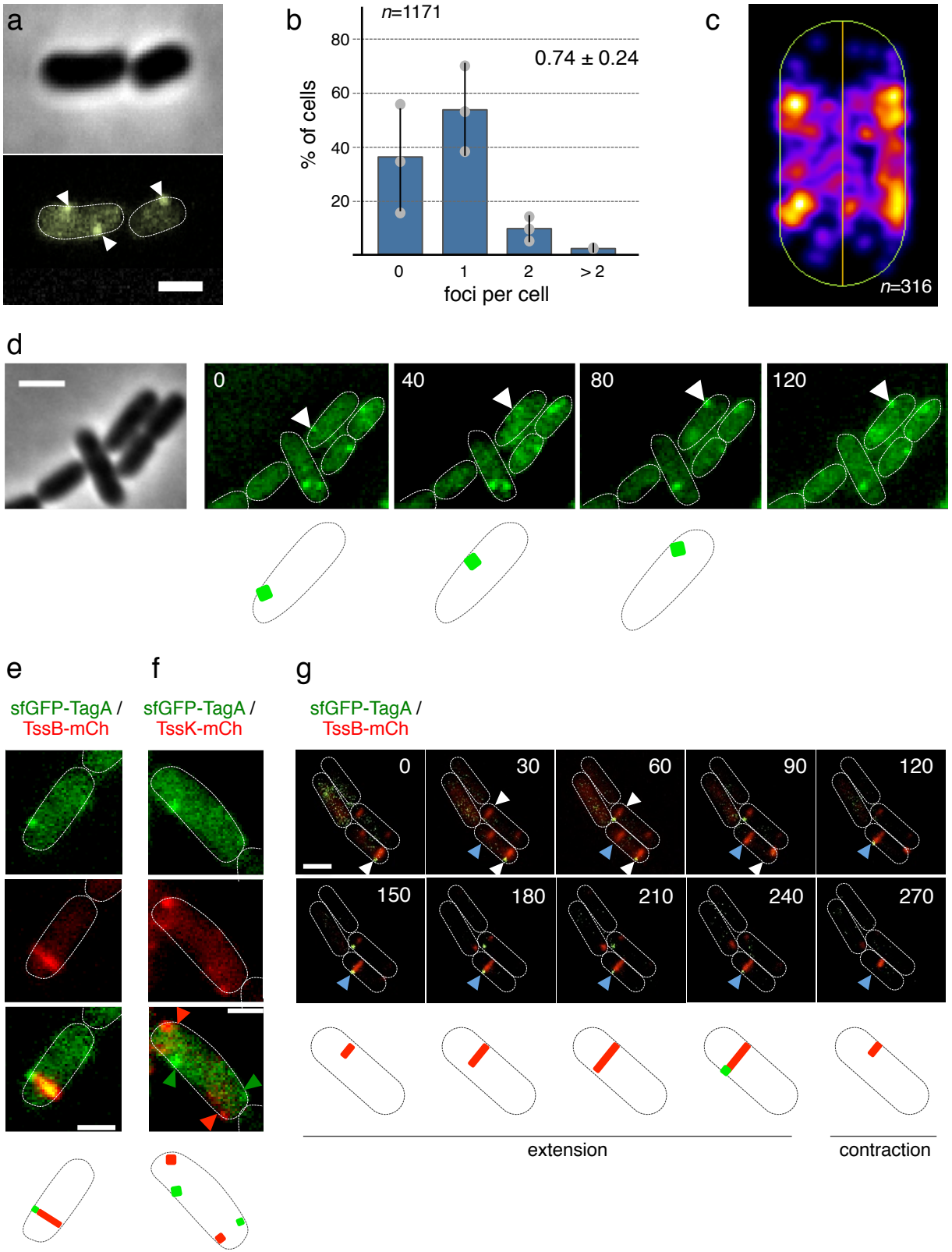
a
b
n=1171
0.74 ± 0.24
% of cells
80
60
40
20
0
1
2
> 2
foci per cell
c
n=316
d
0
40
80
120
e
sfGFP-TagA /
TssB-mCh
f
sfGFP-TagA /
TssK-mCh
g
sfGFP-TagA /
TssB-mCh
0
30
60
90
120
150
180
210
240
270
extension
contraction

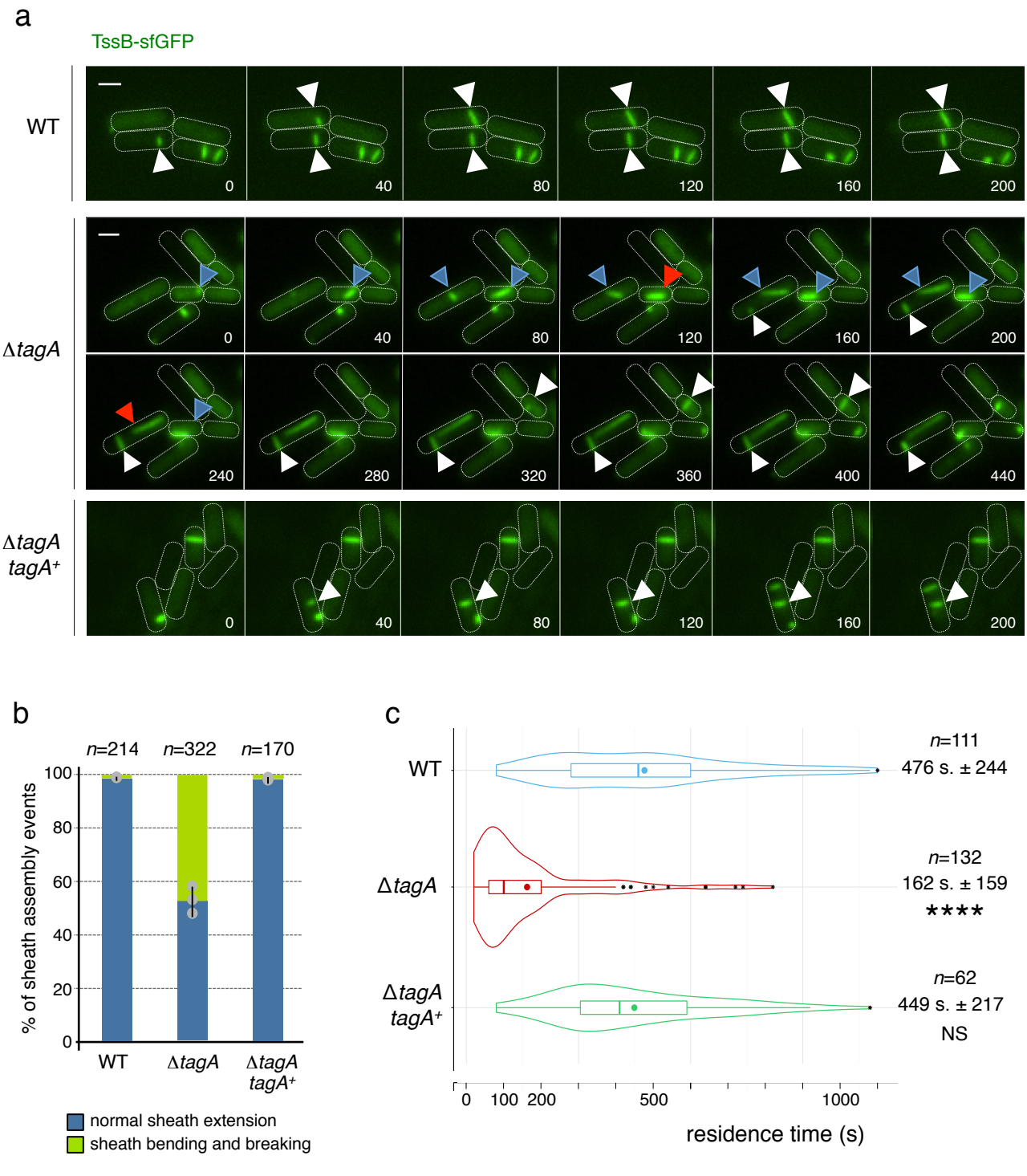
a
TssB-sfGFP
WT
ΔtagA
ΔtagA tagA+
0
40
80
120
160
200
240
280
320
360
400
440
b
n=214
n=322
n=170
% of sheath assembly events
100
80
60
40
20
0
WT
ΔtagA
ΔtagA tagA+
normal sheath extension
sheath bending and breaking
c
WT
ΔtagA
ΔtagA tagA+
n=111
476 s. ± 244
n=132
162 s. ± 159
****
n=62
449 s. ± 217
NS
0
100
200
500
1000
residence time (s)